Tunable contact angle hysteresis by micropatterning surfaces

Damien Debuisson, Vincent Senez, S. Arscott

Tunable contact angle hysteresis by micropatterning surfaces

Cite as: Appl. Phys. Lett. **98**, 184101 (2011); https://doi.org/10.1063/1.3576921
Submitted: 06 January 2011 • Accepted: 20 March 2011 • Published Online: 03 May 2011

Damien Debuisson, Vincent Senez and Steve Arscott

Tunable contact angle hysteresis by micropatterning surfaces

Damien Debuisson, Vincent Senez, and Steve Arscott[a)]
Institut d'Electronique, de Microélectronique, et de Nanotechnologie (IEMN), CNRS UMR-8520, University of Lille, Cite Scientifique, Villeneuve d'Ascq 59652, France

(Received 6 January 2011; accepted 20 March 2011; published online 3 May 2011)

Lithography is used to form circular micropatterns which govern the evaporation of a water droplet. The surfaces are composed of concentric circular defects having a smooth indentation profile. When a droplet encounters a micropattern, evaporation occurs with distinct discontinuities in the droplet wetting contact angle and base radius. The addition of gaps into the patterns enables modification of the contact angle hysteresis; the receding angle of fluorocarbon coated SU-8 can be tuned between 34.6° and 89.1° and that of SU-8 from 5.6° to 43.3° depending on the gap length. A model is developed which accurately predicts the observed behavior. © *2011 American Institute of Physics*. [doi:10.1063/1.3576921]

Wetting[1] is of great scientific interest and has numerous practical applications ranging from the development of new textiles,[2] self-cleaning surfaces,[3] and nanotechnology.[4] Engineering these requires an understanding and control of contact angle hysteresis (CAH),[5–8] i.e., the difference between the advancing contact angle and the receding contact angle of a moving contact line. Here, we study homogenous surfaces containing smooth indentation defects formed by micropatterning a photoresist to control the CAH.

Consider Fig. 1(a) which shows a droplet pinned to a circular "defect"[5] having a radius r_d which contains a gap having a lateral length (x direction) G. Figures 1(b) and 1(c) show side-views of the droplet cut along BB' and CC'. θ^*_{rG} is the contact angle when the droplet depins from the circular defect at points p and p'; we call this the effective receding contact angle for a given G; this is the *minimum* contact angle a droplet can have on such defects. θ_r is the receding contact angle of the droplet on a surface without a circular defect. As we will see, θ^*_{rG} can vary between θ_r ($G=2\pi r_d$) and θ^*_r ($G=0$).[9] Consider the small meniscus formed in the locality of the gap; we have two radii of curvatures: r_2 and r_3, with r_1 being the radius of curvature of the droplet [Fig. 1(b)]. The component of the force in the y-direction F_y is given by

$$F_y = \gamma \int_\Gamma dl \mathbf{e}_y \cdot \mathbf{n} \cos\theta, \tag{1}$$

where γ is the liquid-vapor surface energy, θ is the local contact angle, $\mathbf{n}$ is the unit vector normal to the contact line in the x-y plane, $\mathbf{e}_y$ is the unit vector pointing in the y-direction, l is the arc length parameter of the contact line, and Γ is the contact line which is composed of: (i) a defect pinned portion Γ_d and (ii) a gap associated portion Γ_G. When the droplet depins: $\theta=\theta^*_{rG}$ along Γ_d and $\theta=\theta_r$ along Γ_G. By solving Eq. (1) over the contact line Γ we have

$$F_y = \gamma G(\cos\theta^*_{rG} - \cos\theta_r) \tag{2}$$

by assuming that the depinning of the liquid is independent of G we have a force f_d associated with the defect.[5] Thus, the effective receding contact angle (for a given G) can be written

$$\theta^*_{rG} = \cos^{-1}\left(\frac{f_d}{\gamma G} + \cos\theta_r\right). \tag{3}$$

Note that Eq. (2) is a solution for an arbitrary shaped defect. We can now determine expressions for the radii of curvature of the meniscus. Near to the gap the liquid forms a small meniscus of radius r (in the x-y plane). This radius is the intersection of the sphere of radius r_3 and the x-y plane. Note that r_1 and r_2 are positive while r and r_3 are negative. The Young–Laplace equation[10] allows us to write

$$\frac{2}{r_1} = \frac{1}{r_2} + \frac{1}{r_3}. \tag{4}$$

Thus, in terms of the parameters: r, r_d, θ^*_{rG}, and θ_r, simple geometry can be employed to give the following:

$$r_1 = \frac{r_d}{\sin\theta^*_{rG}}, \tag{5}$$

$$r_2 = \left(\frac{2\sin\theta^*_{rG}}{r_d} - \frac{\sin\theta_r}{r}\right)^{-1}, \tag{6}$$

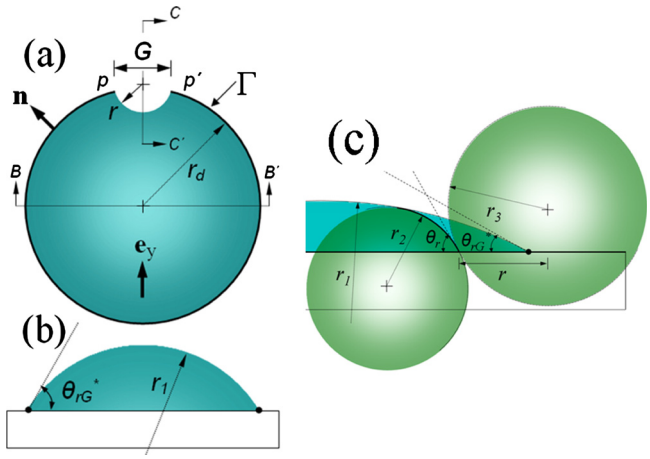

FIG. 1. (Color online) (a) Top view of a droplet pinned to a circular shaped defect of radius r_d having a gap of lateral length G. (b) Cross-section of the same droplet along the BB' plane as indicated in (a). (c) Cross-section of the meniscus formed by the gap along the CC' plane as indicated in (a).

[a)]Electronic mail: steve.arscott@iemn.univ-lille1.fr.

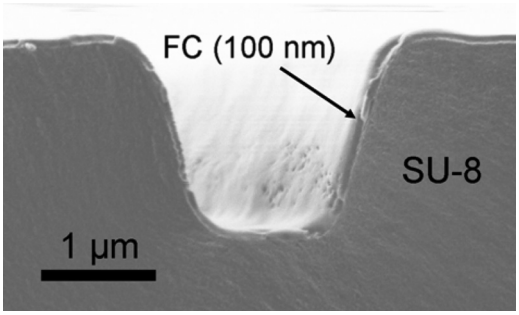

FIG. 2. Scanning electron microscopy image of the cross-section of a smooth trenchlike defect fabricated using photolithography of the photoresist SU-8.

$$r_3 = \frac{r}{\sin\,\theta_r}. \tag{7}$$

In order to test the above reasoning we have fabricated micropatterned smooth defects using lithographic methods. Practical control of CAH can be achieved mesa structures;[7,8] here, we form smooth indentations into the surface. The photoresist SU-8 (Microchem, USA) was used to form circular trenchlike defects; SU-8 is very versatile for microfluidics.[11] The micropatterned surfaces were fabricated on 3 in. diameter silicon wafers (Siltronix, France) using SU-8 2010. The photoresist was spin coated (3300 rpm/1000 rpm s^{-1}/30 s) and prebaked (95 °C for 4 min) which resulted in a thickness of 9.56 μm ($\pm$0.33 μm). The micropatterns were defined using a single photomask; optimized lithography[12] (7.7 s/10 mW cm^{-2}) using a 1 μm linewidth caused Fresnel diffraction underneath the mask[13] which results in the smooth trenchlike defects as show in Fig. 2. Once the SU-8 surfaces had been prepared a fluorocarbon layer (FC) (thickness ~100 nm) could be deposited using a C_4F_8 plasma (STS Ltd., U.K.).

The contact angle measurements were performed using a drop shape analysis system DSA100 (Kruss, Germany). The experiments were performed in a class ISO 5/7 cleanroom (T=20 °C $\pm$ 0.5 °C; RH=45% $\pm$ 2%). A single drop (vol ~2 μl) of de-ionized water was placed over a micropattern using a pipette and allowed to evaporate (unforced).

If there are no gaps in the circles the receding contact angle of such a micropattern has an *effective* receding contact angle θ_r^* which depends on the *profile* of the indentation.[9] It will be seen here that by adding gaps the value of θ_r^* can be modified. The concentric circles had a spacing D of 50 and 100 μm and gap length G which ranged from 20 to

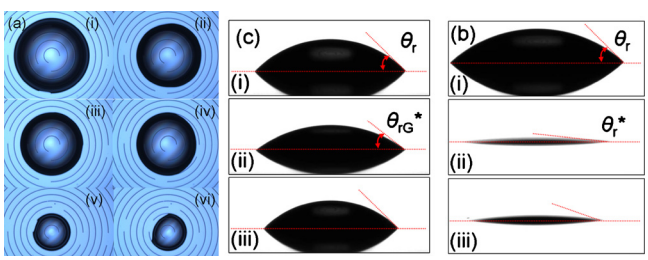

FIG. 3. (Color online) Evolution of the droplet shape as a function of time (a) plan view for H_2O droplet on SU-8 coated with FC surface containing smooth trenchlike circular defects shown in Fig. 2. (Circle spacing D =50 μm, gap length G=100 μm). Effect of gap length on the CAH for (b) D=100 μm, G=0 and (c) D=100 μm, G=50 μm. (b) and (c) are an SU-8 surface smooth trenchlike circular defects.

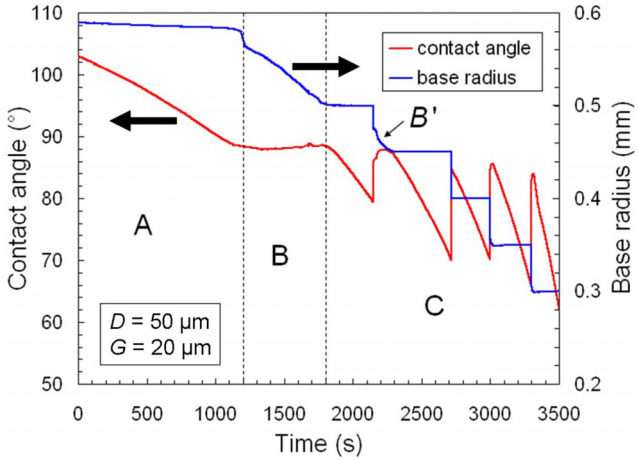

FIG. 4. (Color online) Variation in droplet contact angle and base radius as a function of time for an evaporating droplet (H_2O) on a micropatterned surface (SU-8 coated with FC with D=50 μm and G=20 μm).

200 μm. In each pattern, the largest concentric circle had a diameter of 2 mm; the capillary length[10] $\sqrt{\gamma/\rho g}$ of water (γ=72.8 mJ m^{-2} and ρ=998.2 kg m^{-3})[14] is around 2.7 mm so gravity effects can be ignored in the interpretation of the results. In addition to testing the micropatterns with the gaps we measured the receding contact angle of water on the SU-8 surface used for the study (43.3° $\pm$ 1.6°) and the SU-8 coated with FC (89.1° $\pm$ 2.5°) and on a micropattern without

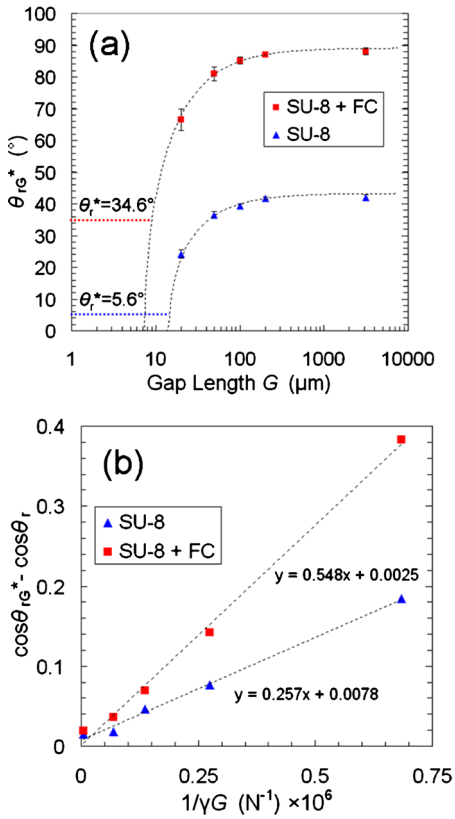

FIG. 5. (Color online) (a) Variation in the effective receding contact angle θ_{rG}^* of the droplet (squares=H_2O on SU-8 coated with FC, triangles=H_2O on SU-8) as a function of gap length G for micropatterned surfaces containing smooth trenchlike defects shown in Fig. 2. The dashed line corresponds to the model [Eq. (3)] by fitting the average defect force f_d calculated from the measurements. (b) A plot of cos θ_{rG}^*−cos θ_r vs the reciprocal of surface tension-gap length product γG. The dashed line represents a simple linear fit.

TABLE I. Summary of results for SU-8.

SU-8	Experimental			Calculated	
G	θ^*_{rG} (deg)	r_1 (μm)	r (μm)	r_2 (μm)	r_3 (μm)
20	24.2($\pm$1.1)	1219.7	−16.8	23.6	−24.5
50	36.5($\pm$0.8)	840.6	−75.7	87.4	−110.4
100	39.3($\pm$0.4)	789.4	−288.7	203.7	−421.0
200	41.8($\pm$0.9)	750.2	−291.0	199.1	−424.3

TABLE II. Summary of results for SU-8 coated with FC.

SU-8+FC	Experimental			Calculated	
G	θ^*_{rG} (deg)	r_1 (μm)	r (μm)	r_2 (μm)	r_3 (μm)
20	66.5($\pm$2.1)	66.5	545.2	−14.9	14.1
50	80.9($\pm$1.1)	80.9	506.4	−87.3	64.9
100	85.1($\pm$0.4)	85.1	501.8	−553.7	172.7
200	87.0($\pm$1)	87.0	500.7	1366.0	306.5

gaps, i.e., closed concentric circles SU-8 ($5.6° \pm 1.3°$) and SU-8 coated with FC ($34.6° \pm 3.4°$).

The evolution of the droplet shape from above [Fig. 1(a)] and plan view [Fig. 1(b)] was recorded as a function of time as the droplet evaporated. At least ten measurements were conducted for each point and error bars are the standard deviation. Analysis of the images allowed us to extract the value of r at the moment of droplet depinning from the circular pattern initially at points p and p' [Fig. 1(a)].

Figure 3 shows optical microscope images of the evolution of the water droplet shape (plan view) as a function of time (~80 s). The micropattern here is concentric circles spaced at a distance equal to 50 μm and a gap equal to 100 μm. The surface is SU-8 coated with 100 nm of FC. The recorded times between the images are 20 s for (i)–(iii) and 60 s between (iv) and (v). In contrast, the droplet depinning, see the transitions from (i) to (ii), (iii) to (iv), and (v) to (vi), occurs over a relatively short period in <200 ms). Figures 3(b) and 3(c) show the evolution of the droplet profile (side-view) as a function of time for two different values of G. As the droplet evaporates it becomes pinned on a circular defect with a meniscus forming around the gap. As the contact line moves down the trenchlike defect, the effective contact angle diminishes at constant base radius.[9] At the moment of depinning, the droplet depins from the gap at points p and p' [Fig. 1(a)] and evaporates further to pin onto a smaller concentric circle, the process repeating itself until full evaporation of the water.

Figure 4 shows plots of the droplet contact angle and base radius as a function of time. The two well-known evaporation phases[15] are visible indicated as A and B (Fig. 4). The first phase A corresponds to evaporation at constant droplet base radius with reducing contact angle while the second phase B corresponds to reducing droplet base radius at constant contact angle. These two phases are observed until the contact line portion Γ_d is entirely pinned to a single circle defect. Once the droplet is pinned, a phase C is observed, where the contact angle and the base radius of the droplet evolve in distinct jumps and steps, respectively, as the droplet pins to and depins from successive circular defects. Note that the phase[15] B' (Fig. 4) corresponding to the initial droplet depinning from a circle (r_d=0.5 mm) finishes *between* two circular defects as the droplet depins at a larger contact angle than θ^*_{rG} due to a surface impurity. The relationship between the droplet base radius and the droplet contact angle in phase C has been given by the authors.[9] Modeling of flat *heterogeneous* surfaces[6] predicts contact angle jumps and a reduction in contact angle as the droplet size becomes small; both effects are observed here but on a chemically *homogenous* surface containing smooth defects.

Figure 5(a) shows plots of θ^*_{rG} as a function of G for the two different surfaces measured (SU-8 and SU-8 coated with FC). Equation (3) is also plotted in Fig. 5(a) using the value of f_d extracted from the measurements and the value of θ_r measured on flat surfaces. The value of f_d was calculated from the data to be 534.4 nN$\pm$9.5 nN and 283.7 nN$\pm$14.9 nN for SU-8 coated with FC and SU-8, respectively. As G increases then the value of θ^*_{rG} tends to θ_r. However, as the value of G diminishes clearly our model does not predict the value of θ^*_r for a circle having G=0; $5.6° \pm 1.3°$ in the case of SU-8 and $34.6° \pm 3.4°$ in the case of SU-8 coated with FC.[9] The physical reason for this is that the value of θ^*_{rG} cannot be smaller that the value measured on a closed concentric circle (G=0). Thus in reality, θ^*_{rG} will follow the horizontal dashed lines (red and blue) [Fig. 5(a)]. In this way we are able to predict the minimum value of G which can have an influence on the value of θ^*_{rG}; this value is 9 μm for SU-8 coated with FC and 14.5 μm for SU-8, for the defect profile studied here. A plot of $\cos\theta^*_{rG} - \cos\theta_r$ versus $1/\gamma G$ [Fig. 5(b)] reveals a straight line passing through the origin which is predicted by our model; a simple linear fit to the data yields a defect force f_d of 548 nN and 257 nN on SU-8 coated with FC and SU-8, respectively. Note that f_d is larger on SU-8 coated with FC than on SU-8 which is more hydrophilic. This is because f_d is linked to the CAH induced by a defect on the receding contact angle and not to the wettability. Thus, the origin of f_d has more complex causes, e.g., the surface roughness and the liquid micromeniscus behavior.[5] By measuring the value of the meniscus radius r [Fig. 1(c)] at the moment of depinning and knowing the value of θ^*_{rG} one can calculate the values of the radii of curvature [Fig. 1(c)] at each value of G on a given surface (for r_d=0.5 mm). Tables I and II present numerical results of the study.

[1] D. Quéré, Mater. Res. **38**, 71 (2008).
[2] X. J. Feng and L. Jiang, Adv. Mater. (Weinheim, Ger.) **18**, 3063 (2006).
[3] R. Blossey, Nature Mater. **2**, 301 (2003).
[4] J. B. Hannon, S. Kodambaka, F. M. Ross, and R. M. Tromp, Nature (London) **440**, 69 (2006).
[5] J. F. Joanny and P. G. De Gennes, J. Chem. Phys. **81**, 552 (1984).
[6] H. Kusumaatmaja and J. M. Yeomans, Langmuir **23**, 6019 (2007).
[7] M. Reyssat and D. Quéré, J. Phys. Chem. B **113**, 3906 (2009).
[8] J. W. Krumpfer and T. J. McCarthy, Faraday Discuss. **146**, 103 (2010).
[9] D. Debuisson, R. Dufour, V. Senez, and S. Arscott (unpublished).
[10] P. G. de Gennes, Rev. Mod. Phys. **57**, 827 (1985).
[11] J. Carlier, S. Arscott, V. Thomy, J. C. Fourier, F. Caron, J. C. Camart, C. Druon, and P. Tarbourier, J. Micromech. Microeng. **14**, 619 (2004).
[12] M. Gaudet, J. C. Camart, L. Buchaillot, and S. Arscott, Appl. Phys. Lett. **88**, 024107 (2006).
[13] Y. Cheng, C.-Y. Lin, D.-H. Wei, B. Loechel, and G. Gruetzner, J. Microelectromech. Syst. **8**, 18 (1999).
[14] *CRC Handbook of Chemistry and Physics*, 69th ed., edited by R. C. Weast (CRC Press, Florida, USA, 1988).
[15] R. G. Picknett and R. Bexon, J. Colloid Interface Sci. **61**, 336 (1977).